ACS Chemical Neuroscience
Cite This: ACS Chem. Neurosci. 2019, 10, 1744−1752
Research Article
pubs.acs.org/chemneuro

Ultrafast Glutamate Biosensor Recordings in Brain Slices Reveal Complex Single Exocytosis Transients

Yuanmo Wang,[†] Devesh Mishra,[‡,⊥] Jenny Bergman,[∥] Jacqueline D. Keighron,[†] Karolina P. Skibicka,[⊥,‡] and Ann-Sofie Cans*[,†]

[†]Department of Chemistry and Chemical Engineering, Chalmers University of Technology, Kemigården 4, SE-412 96 Gothenburg, Sweden

[‡]Department of Physiology/Metabolic Physiology, Institute of Neuroscience and Physiology, The Sahlgrenska Academy at the University of Gothenburg, Medicinaregatan 11, SE-413 90 Gothenburg, Sweden

[∥]Department of Chemistry and Molecular Biology, University of Gothenburg, Kemigården 4, SE-412 96 Gothenburg, Sweden

[⊥]Wallenberg Centre for Molecular and Translational Medicine, University of Gothenburg, SE-405 30 Gothenburg, Sweden

Supporting Information

ABSTRACT: Neuronal communication relies on vesicular neurotransmitter release from signaling neurons and detection of these molecules by neighboring neurons. Glutamate, the main excitatory neurotransmitter in the mammalian brain, is involved in nearly all brain functions. However, glutamate has suffered from detection schemes that lack temporal and spatial resolution allowed by electrochemistry. Here we show an amperometric, novel, ultrafast enzyme-based nanoparticle modified sensor, measuring random bursts of hundreds to thousands of rapid spontaneous glutamate exocytotic release events at approximately 30 Hz frequency in the nucleus accumbens of rodent brain slices. Characterizing these single submillisecond exocytosis events revealed a great diversity in spike shape characteristics and size of quantal release, suggesting variability in fusion pore dynamics controlling the glutamate release by cells in this brain region. Hence, this novel biosensor allows recording of rapid single glutamate exocytosis events in the brain tissue and offers insight on regulatory aspects of exocytotic glutamate release, which is critical to understanding of brain glutamate function and dysfunction.

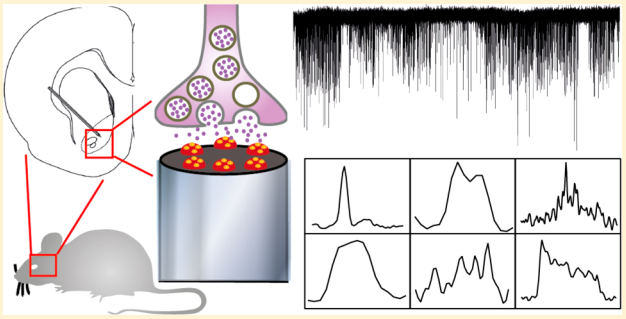

KEYWORDS: *Glutamate, biosensor, ultrafast, glutamate oxidase, gold nanoparticle, microelectrode, amperometry, exocytosis, fusion pore, dynamics, brain slice, rodent, nucleus accumbens*

Glutamate is the most prevalent excitatory neurotransmitter in the mammalian central nervous system (with more than half of all the brain synapses releasing glutamate).[1] It is deemed necessary for all life functions, and dysfunctional glutamate system is thought to underlie many diseases including many neurological and psychiatric disorders.[2−5] For in depth understanding of glutamatergic function, methods able to capture the rapid exocytosis events of vesicular glutamate release from neuronal activity in the brain are sorely needed. Current techniques for monitoring neurochemical activity are based on electrochemical methodology, with amperometry being most commonly used because it is simple to implement and offers outstanding time resolution down to submillisecond time scale. This temporal resolution is fast enough to capture the rapid transients of neurochemical release from single exocytosis events. In comparison with other neurotransmitter molecules that are electroactive such as dopamine, a major issue in measuring glutamate electrochemically is that it is nonelectroactive. To overcome this challenge, recent advances in glutamate amperometry have used glutamate oxidase (GluOx) to convert glutamate to a detectable reporting molecule. While a high degree of specificity has been reached, the desired time resolution for glutamate sensors remains elusive. Current glutamate sensors offer a temporal resolution down to subseconds, which is far too slow for monitoring real-time exocytotic activity,[6] although a methodology with a similar approach to this work showed a glutamate recording that temporally resolved single exocytosis events at a single neuron cultured *in vitro*.[7] We recently developed a new approach for sensor design, which dramatically improves the temporal resolution by minimizing the distance that the electrochemical enzyme product needs to diffuse for sensor detection.[8]

Following this minimal distance principle, we fabricated an ultrafast sensor for glutamate by immobilizing a monolayer coating of GluOx on the surface of gold nanoparticle (AuNP)

Received: November 11, 2018
Accepted: January 3, 2019
Published: January 3, 2019

DOI: 10.1021/acschemneuro.8b00624
ACS Chem. Neurosci. 2019, 10, 1744−1752

modified carbon fiber microelectrode. Using this strategy and placing the sensor probe in the nucleus accumbens (NAc) of rodent brain slice, we were able to achieve an unparalleled temporal resolution of measuring bursts of individual glutamate transients during spontaneous glutamate release in the brain tissue. These current spikes corresponding to single-vesicle exocytosis events revealed a variety in size and current spike shape characteristics indicating synaptic tuning of glutamate on the single vesicle level. In summary, our approach is able to record exocytosis activity with submillisecond temporal resolution, such that individual current spikes can be related to single exocytosis events. Therefore, it allows us to monitor and characterize the fusion pore dynamics regulating glutamate release at the single exocytosis event level.

RESULTS AND DISCUSSION

To increase temporal resolution for glutamate recordings and to achieve resolution capable of capturing glutamate activity in brain tissue at the single-exocytosis level, we fabricated and utilized a specific sensor design scheme (Figure 1). Briefly, the

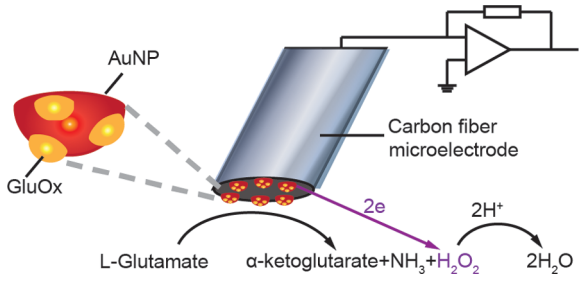

Figure 1. Schematic of the amperometric glutamate sensor design consisting of a GluOx-coated gold nanoparticle modified carbon fiber microelectrode. It displays the chemical enzyme catalysis reaction chain for glutamate with the subsequent detection scheme for electrochemical detection of the reporter molecule H_2O_2 produced. The red hemispheres represent gold nanoparticles and the enzyme glutamate oxidase that is immobilized at the surface is displayed in yellow. Schematics are not drawn to scale. The chemical enzyme catalysis reaction chain for glutamate with the subsequent detection scheme for electrochemical detection of the reporter molecule H_2O_2 produced is displayed in the figure.

sensor was functionalized by electrochemically depositing AuNP hemispheres onto a 33-μm diameter carbon fiber disc microelectrode, and subsequently immobilizing a mono layer of GluOx onto it. The optimal conditions for forming a GluOx monolayer were determined using analytical methods to carefully characterize the GluOx interaction with the AuNP surface (Figure 2). This ultrathin enzyme layer was critical for converting glutamate into α-ketoglutarate,[3,6] and in minimizing the diffusion time of the enzyme product hydrogen peroxide (H_2O_2) to reach the sensor surface for detection, thereby increasing the temporal resolution of the sensor.[8] The electrochemically deposited gold nanoparticle hemispheres at the sensor surface (1) offer a larger sensor surface area for enzyme immobilization, (2) provide a high surface curvature that prevents enzyme denaturation and associated loss of enzyme activity,[9,10] and (3) enable the detection of the reporter molecule H_2O_2 by recording the reduction current at a potential of −0.5 V at the sensor surface vs a Ag/AgCl reference electrode.

Improving Glutamate Sensor Speed by Minimizing the Enzyme Coating Thickness. We used a flocculation

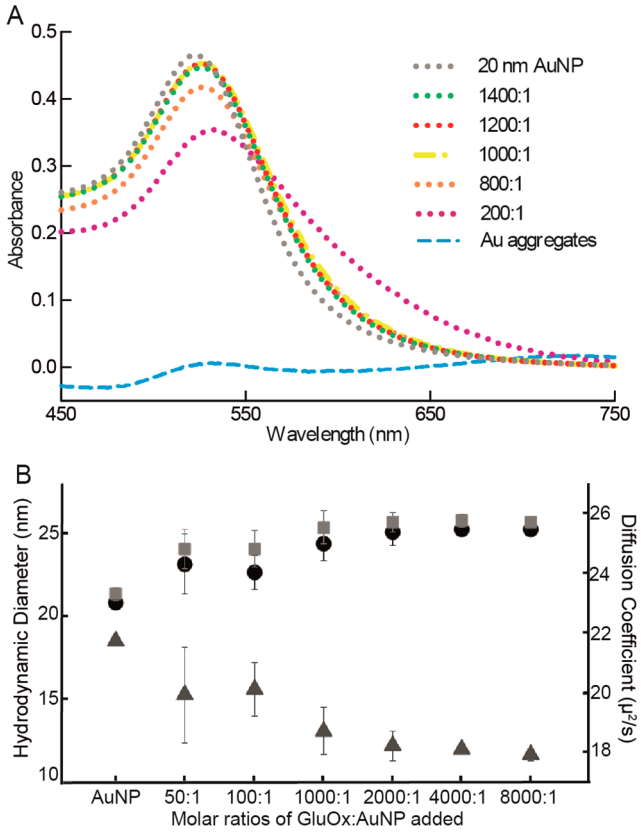

Figure 2. Analytical methods were used to determine the conditions needed for immobilization of enzyme to create a complete monolayer coverage of enzyme at the AuNP modified sensor surface. (A) Absorption spectrum of GluOx:AuNP conjugates from flocculation assays investigating molar ratios of GluOx versus AuNP needed (from 200:1 to 1400:1) during the conjugation process to cover a 20 nm in diameter AuNP surface. The enzyme:AuNP conjugate peak spectra that overlap with the plasmonic peak of bare AuNP in solution indicate AuNP with a full enzyme coverage and red peak shift as seen for spectra of AuNP aggregates mark incomplete enzyme coverage. (B) The resulting hydrated diameter (D_{hyd}) of GluOx-AuNP conjugates and of bare 20 nm AuNP was measured using DLS (circles, attenuation, n = 9) with its corresponding diffusion coefficient (triangles) and NTA (squares, n = 9). The measurements were carried out at room temperature (22 °C) ~ 6 h after conjugate formation. Error bars are expressed as standard deviation of the mean values.

assay to determine the optimal GluOx concentration for coating a thin monolayer of enzyme at the AuNP surface. Here, only conjugates where the enzyme fully coats the AuNP surface will remain sterically protected from flocculation when subjected to high salt conditions. To find the minimal GluOx concentration to achieve monolayer coverage on AuNP, we titrated different molar ratios of GluOx to AuNP (20 nm in diameter) in bulk solution while monitoring the conjugate stability using spectrophotometry. The assay showed that at molar ratios from 800:1 (GluOx:AuNP) and above, stable enzyme GluOx-AuNP conjugates were formed as displayed by the spectral overlap with the plasmonic peak for bare AuNP (Figure 2A), whereas at lower molar ratios, a redshift of the plasmonic peak indicates formation of gold aggregates (Figure 2A). To verify the resulting thickness of the immobilized enzyme at the AuNP surface after conjugation, we measured the hydrodynamic diameter, D_{hyd} of the conjugates using

DOI: 10.1021/acschemneuro.8b00624
ACS Chem. Neurosci. 2019, 10, 1744−1752

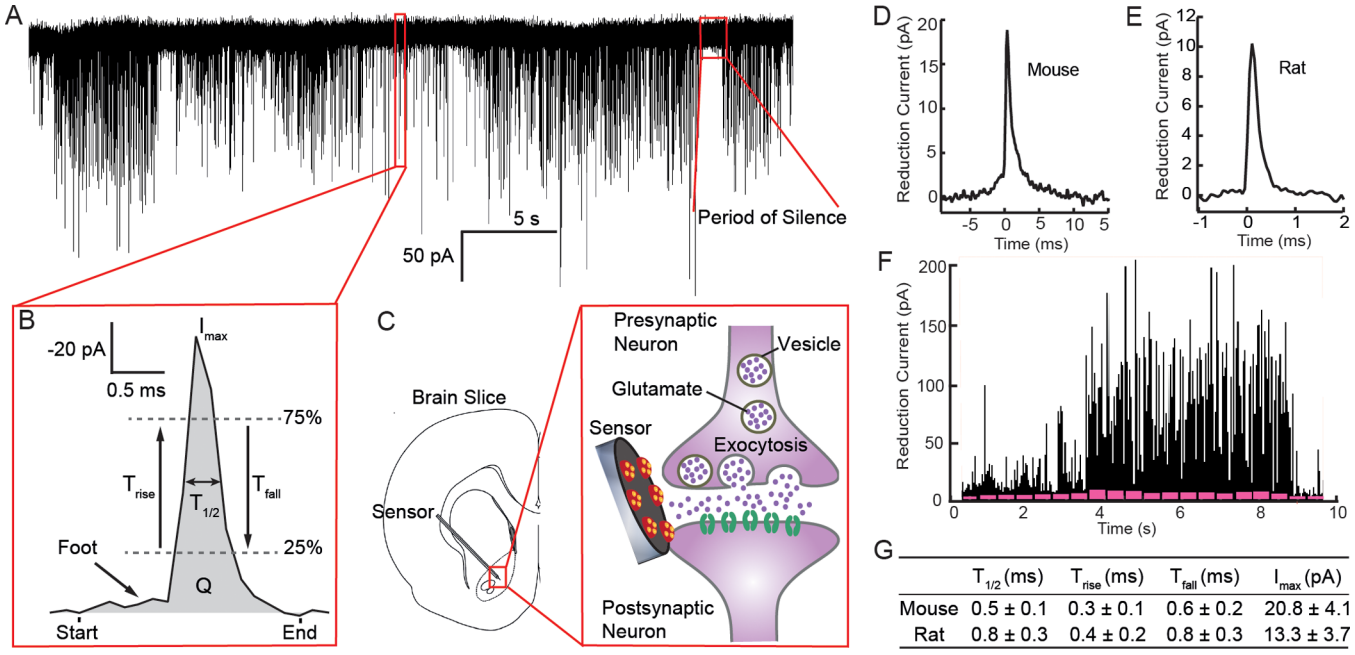

Figure 3. (A) Amperometric current–time trace detecting bursts of individual exocytosis events during spontaneous glutamate release in mouse brain slice. (B) Definition of the current spike parameters used for exocytosis kinetic analysis after converting the amperometric recording to positive reduction current. (C) Illustration of the placement of sensor in the nucleus accumbens of rodent brain slice for amperometric recording. Schematics are not drawn to scale. (D) and (E) Averaged reduction current transients of single synaptic glutamate release in mouse and rat brain slice, respectively. (F) Glutamate synaptic response sampled at 10 kHz (black) compared to a recalculated amperometric time trace if recorded at 2 Hz (pink). (G) Kinetic analysis of single peak parameters of 4932 and 647 spikes from 7 amperometric recordings in mouse (n = 5) and 4 measurements in rat (n = 2), respectively. The values are shown as the means of means for the total number of measurements ± standard error of the mean (SEM).

dynamic light scattering (DLS) and nanoparticle tracking analysis (NTA). Both NTA and DLS measurements (Figure 2B) showed that increasing the molar ratio of enzyme:AuNP up to 1000:1 resulted in increased size of the conjugates, but further increases in enzyme concentration did not cause additional changes in the size of the conjugates. In addition, further addition of enzyme resulted in a narrower distribution in conjugate size, as a larger amount of enzyme provides enough material to fully coat the surface of all AuNP in the sample. This indicates that by adding enzyme:AuNP ratios of 4000:1 or higher, a complete enzyme monolayer is formed at the surface of the majority of AuNPs solution, whereas using a 8000:1 ratio, we were able to fully coat all AuNP in the sample while forming a fully stable enzyme monolayer of GluOx-AuNP conjugates.

In addition, to verify the DLS measurements, the measured diffusion coefficient of GluOx-AuNP conjugates confirmed that the conjugate size increases with molar ratios added up to 1000:1. At higher enzyme ratios, the conjugate size remains constant, which supports the idea that GluOx forms monolayer, rather than a multilayer at the AuNP surface. Therefore, to ensure immobilization of a complete and ultrathin layer of enzyme at the sensor surface during fabrication and to compensate for potential loss of enzyme during the enzyme immobilization process due to adsorption to for instance the glass wall that insulates the sensor surface, the tip of the electrode was incubated in a GluOx solution with an excess amount of enzyme that is needed to form monolayer coatings. Post fabrication, the glutamate sensor was tested in bulk solutions and characterized in terms of sensitivity and selectivity. At this potential, our sensor could detect 10 μM glutamate (Supporting Information Figure S1A), while avoiding majority of oxidative interferents and displaying good selectivity against common interferents like dopamine in NAc (Supporting Information Figure S1B,C).

Spontaneous Glutamate in Rodent Brain. To test the efficiency of the glutamate measurements, we applied our sensor to coronal rodent brain slices by placing the sensor in the NAc area (Figure 3C), a brain region controlling goal-directed behavior. NAc region is mainly regulated by glutamatergic inputs from, for example, prefrontal cortex, basolateral amygdala, hippocampus and hypothalamus, and by dopaminergic inputs from the ventral tegmental area.[11−15] Abnormal plasticity in these glutamatergic pathways underlies the course of drug-addiction.[16,17] Using this strategy, we were able to achieve an unparalleled temporal resolution of measuring single-vesicle exocytosis events during spontaneous glutamate release. A representative amperometric-time trace of reduction spikes corresponding to the detection of serial bursts of glutamate release is displayed in Figure 3A. Recordings in rat (n = 4) and mouse (n = 4) of spontaneous burst of glutamate activity showed an average frequency of 28.6 ± 10.7 Hz and 27.9 ± 11.5 Hz, respectively (error representing the standard error of mean), which is in line with activity levels previously reported from glutamate electrophysiology recordings.[18,19] These bursts of glutamate exocytosis activity were often followed by a short period of silence of 2.8 ± 0.8 s (mouse) and 3.5 ± 1.2 s (rat) and were comprised of numerous smaller sub clusters of current spikes, respectively. Each burst covered hundreds to thousands of individual rapid submilliseconds to milliseconds current transients, where each spike was related to glutamate release from a single vesicle exocytosis event. The representative averaged single spike from recorded reduction spikes in mouse (n = 3297) and rat (n =

DOI: 10.1021/acschemneuro.8b00624
ACS Chem. Neurosci. 2019, 10, 1744−1752

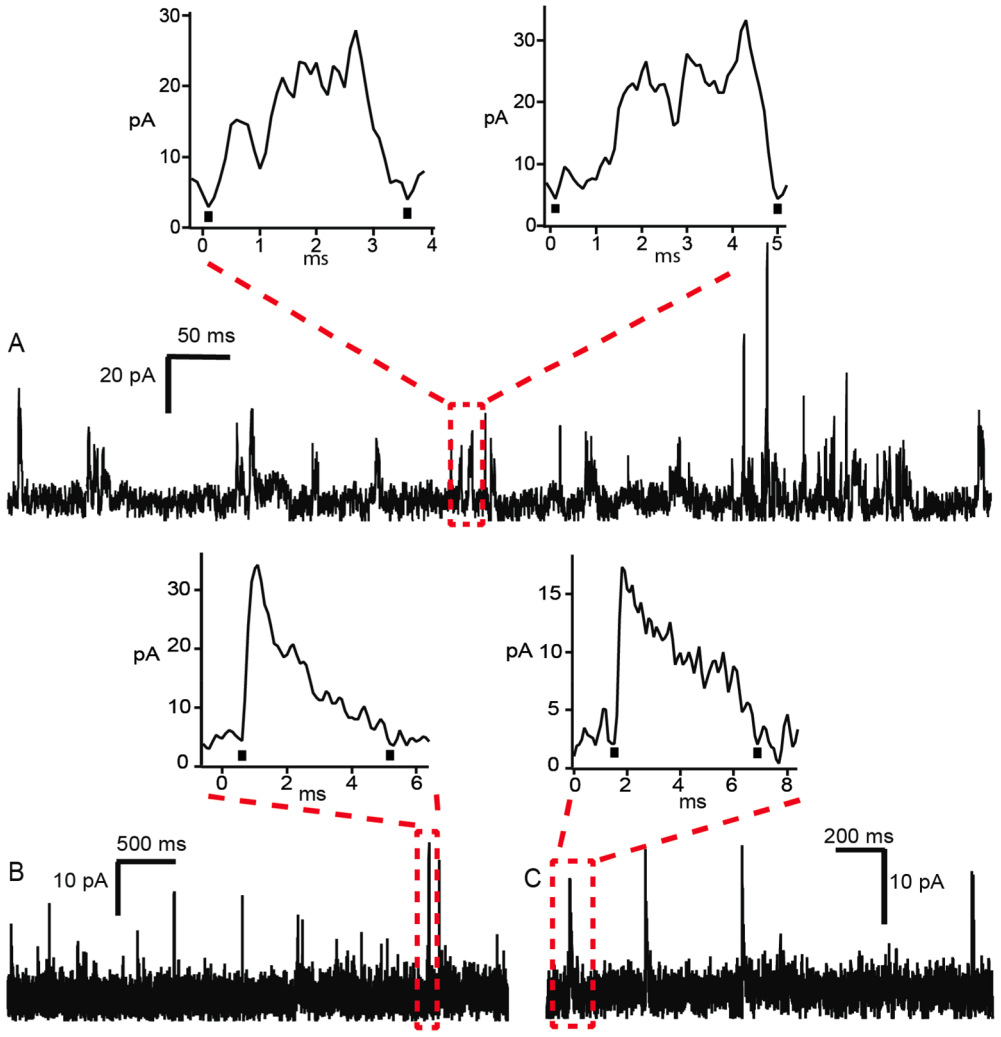

Figure 4. Representative amperometric traces of complex exocytotic spike events isolated from the recorded amperometric baseline, with inserts showing a close up of isolated spikes that were categorized as (A) "increasing plateau" events and (B) and (C) as "decreasing plateau" events.

409) brain slices are shown in Figure 3D,E. Both the current spike shape characteristics and kinetics of glutamate transients with half-time decay on submilliseconds time scale support the sensor's ability to resolve single synaptic vesicle exocytosis events.[20−22] Hence, if commonly used recording speed of 2 Hz was used compared to 10 kHz used here, both the information on neuronal activity and exocytosis dynamics would be missing (Figure 3F). Summarized temporal dynamics of individual spike kinetics in Figure 3B,G show a sharp current rise time, a slower decay with half-time decay on submilliseconds time scale. This suggests (1) the onset of exocytosis from an expanding fusion pore and (2) a slower decay representing diffusion limited glutamate transport from the fusion pore release site to the electrode surface. That we do not observe diffusional broadening of the current transients, suggests our sensor is positioned very close to the glutamate release site.[20,23,24]

In addition, the high temporal resolution of the spontaneous glutamate activity enabled by our recordings, indicated a diversity of shape and time courses for single spikes. This implies that glutamate release is regulated by factors controlling the dynamics of fusion pore opening and closing during the exocytosis process. Figure 4 presents examples of a couple of the complex spikes that were isolated from the recorded current background baseline, and a summary of all different types of detected spikes and their abundance in recordings is presented in Figure 5. These different type of spikes categorized by shape and kinetics are similar to previous reported recordings of octopamine release in *Drosophila melanogaster* tissue.[25] This supports previous observations of heterogeneous glutamate release at ribbon type synapses.[26,27] Each spike category was replicated between the mouse and the rat recording. The most commonly detected spike in vesicle exocytosis events is initiated with a rapid current rise followed by a slow decay (Figure 5A); it accounts for 52.9% (mouse) and 44.1% (rat) of all spikes detected. A current prespike "foot" was frequently observed prior to the rapid rise at these current transients, indicating that the exocytosis event is initiated by formation of a nanometer-sized fusion pore from which glutamate is leaking before the pore further dilates and expels a larger amount of glutamate as previously also noted by synaptic glutamate release at goldfish retinal bipolar cells.[21,26] Apart from the occurrence of double or triple peaks that most likely correspond to codetection of simultaneous exocytosis events with spatial and temporal overlap (Figure 5B), other common categories of spikes were characterized by a fast rise with steady decrease in current amplitude (Figure 5F) or a broader type where the current steadily increase with time until

DOI: 10.1021/acschemneuro.8b00624
ACS Chem. Neurosci. 2019, 10, 1744−1752

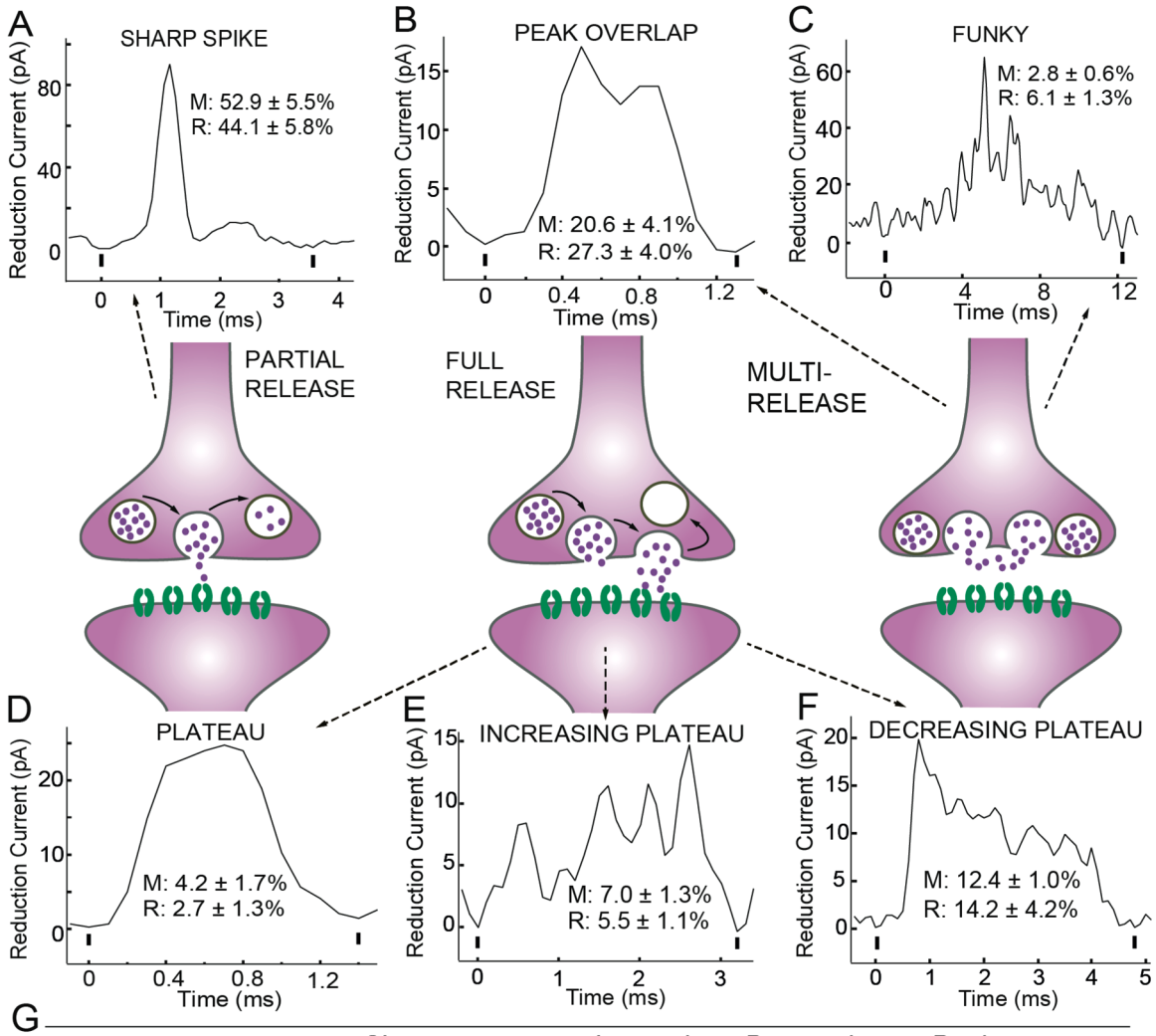

G

	Spike Types	Sharp Spike	Plateau	Increasing Plateau	Decreasing Plateau	Peak Overlap	Funky
Mouse	Charge (fC)	10.2	16.0	14.7	17.0	16.0	38.8
	SEM (fC)	3.8	6.8	6.3	7.2	6.8	20.7
	Percentage (%)	69	109	100	115	108	263
Rat	Charge (fC)	8.7	11.9	14.0	15.3	11.9	27.5
	SEM (fC)	0.8	1.5	2.3	1.5	1.5	4.2
	Percentage (%)	62	85	100	110	85	197

Figure 5. Synaptic glutamate transients (n = 937) and (n = 647) collected from 5 and 4 recordings in mouse (n = 5) and rat (n = 2), respectively, and where all current transients recorded were sorted into 6 categories of spikes. (A)−(F) Representative peaks and frequency for each type of spikes as recorded in rat (R) and mouse (M). (A) The sharp spike is the most commonly detected spike in vesicle exocytosis events, it is initiated with a rapid current rise followed by a slow decay and often preceded by a prespike current "foot". (B) Spikes displayed with shape characteristics of "peak overlap" by double or triple peaks most likely correspond to codetection of simultaneous exocytosis events with spatial and temporal overlap. (C) Current transients that display a more complex shape and that last longer than spikes from the other five categories were all clustered to the group called "funky". (D) Plateau current spikes were characterized by a rapid rise followed by a constant current before a fast decay back to baseline. (E) Spikes that displayed a broader type of spike with a steadily increase in current versus time until an abrupt decay were categorized as "increased plateau". (F) The broader spikes displaying a with fast rise followed by a steady decrease in current amplitude were categorized as "decreasing plateau". (G) Quantitative analysis of the charge and the relative charge value for each category of spike from recordings of glutamate release in mouse and rat.

an abrupt decay (Figure 5E). This kind of exocytotic release might indicate glutamate release through a synaptic fusion pore where the pore size is increasing or decreasing and sometimes during a continuous flickering before the pore closes. Another prevalent spike shape demonstrated was a plateau current (Figure 5D) characterized by a rapid rise followed by a constant current before a fast decay back to baseline, which implies that the fusion pore rapidly opens up to a larger size and stabilizes for a period of time before closing. In addition, current transients that display a more complex shape and that last longer than spikes from the other five categories were identified in our recording, which we here refer to as "funky"

DOI: 10.1021/acschemneuro.8b00624
ACS Chem. Neurosci. 2019, 10, 1744−1752

spikes (Figure 5C). As the integrated charge (Q) from a current spike as defined in Figure 3B, is proportional to the amount of glutamate released, quantification of charge defines the quantal size of exocytotic glutamate release. As summarized in Figure 4G, normalizing the charge detected from all categories of spikes to the charge detected by the spikes with "increasing plateau" shape, shows that all three different kinds of plateau shaped spikes display similar quantal size of glutamate released. In contrast, the sharp spike only detects 2/3 of the normalized quantal size, and funky spikes detect 2−3 times this amount. This indicates that the quantal release detected by the three different plateau shaped spikes signify glutamate release by full exocytosis, whereas the fractional charge detected by the sharp spikes might be derived from a mode of exocytosis where only part of the vesicle content is released, which also is supported by the typical spike shape characteristics observed previously during partial release in other cell types.[28] The peak overlap and funky spikes suggest codetection of two or more vesicles bursting simultaneously or possibly related to compound exocytosis, if this mode of release is present in the glutamatergic terminals projecting to NAc.[29,30] Hence, the variety of current spike shape characteristics and the variability in quantal size of glutamate release suggest the presence of a regulatory machinery controlling the size, dynamics and lifetime of synaptic vesicle fusion pore during exocytosis and that a variety of release mechanisms may be utilized during neuronal activity or potentially also be related to release mechanisms by glial cells[31] and astrocytes[32] in the NAc of rodent brain tissue.

In summary, we here show the effects of limiting the enzyme thickness at the nanoparticle-coated sensor surface to a monolayer, which now also has been supported by optimization modeling.[33] By bringing this new concept in sensor design,[8] applying analytical methods to carefully characterize the GluOx interaction with AuNP and finding the optimal conditions for GluOx monolayer formation at the AuNP surface, we developed an ultrafast glutamate biosensor and recorded spontaneous glutamate activity in the NAc of *ex vivo* rodent brain slice. Employing this sensor for the first time opens up the possibility to temporally resolve fluctuations of glutamate transients on the submillisecond time scale that allows for the monitoring of fusion pore dynamics regulating glutamate release at the level of single exocytosis events. In these recordings, we have been able to categorize a variety of different current spike shapes that suggest various modes of exocytosis release are utilized by these glutamatergic neurons during spontaneous glutamate release. We found spontaneous glutamate events in brain slices occurring with an approximate frequency of 30 Hz, which is in line with activity levels previously reported from glutamate electrophysiology recordings.[18,34] This is of great importance for understanding the role of glutamate in brain function and malfunction, it also has profound implications for future *in vivo* studies in freely behaving animals. Hence, we perceive this as an important step toward measuring glutamate release in freely behaving rodent models, which is our immediate future endeavor. This ultrafast senor may help to finally understand glutamate neurotransmission in neurological states of diseases and health.

METHODS

Materials. L-Glutamate oxidase (GluOx, 5 U) lyophilized powder from *Streptomyces sp.*, sodium chloride (NaCl), sodium bicarbonate ($NaHCO_3$), gold chloride trihydrate, ferrocene-methanol, Whatman Anotop 25 syringe filters with 20 nm filtering size, phosphate-buffered saline tablets (10 mM, pH 7.2), sulfuric acid, copper sulfate, tetrachloroaurate, dopamine chloride, glutamine, glucose, monosodium glutamate, acetylcholine chloride, ascorbic acid, ferrocene methanol (FcMeOH), glycerol, potassium chloride, sodium phosphate, calcium chloride, magnesium chloride, sodium bicarbonate, tungsten wire and hydrogen peroxide were purchased from Sigma-Aldrich (St. Louis, MO, U.S.A.). A 20 nm gold nanoparticle (AuNP) colloidal solution was purchased from BBI Solutions (Cardiff, UK). Milli-Q water with resistivity ≥18 MΩ·cm was used in all experiments.

Enzyme−AuNP Conjugation. For the formation of GluOx-AuNP conjugates, a bottle of L-glutamate oxidase lyophilized powder (5 U) was carefully dissolved in 300 μL of 10 mM sodium bicarbonate (pH 8.2), and the absorption spectrum of the solution was measured using a Cary 4000 or Cary 5000 UV−vis spectrophotometer (Agilent Technologies, U.S.A.) to determine the GluOx concentration. The absorption spectrum of GluOx solution shows three peaks at 273, 385, and 465 nm with molar absorption coefficients of 253 000, 22 000 and 19 000, respectively[35] which can be used to determine the enzyme solution concentration via Beer−Lambert Law (i.e., $A = \varepsilon * l * c$, where A is the value of absorbance, ε is the molar extinction coefficient of a molecule at a specific wavelength, in units of $M^{-1}cm^{-1}$, l is the optical path length over sample, c is the sample concentration). To a fixed volume of 1 nM AuNP solution (monodisperse, 20 nm in diameter), different molar ratios of enzyme were added in a 2 mL Maxymum Recovery centrifuge tube (Maxyclear Boil Proof, VWR, U.S.A.) where enzyme, through self-adsorption, binds to the AuNP surface and forms the GluOx-AuNP conjugates. Sodium bicarbonate buffer solution was used to adjust the final volume of the conjugate samples. During conjugate formation, all samples were incubated in the dark for 1.5 to 2 h at the room temperature. Thereafter, the isolation of GluOx-AuNP conjugates was performed by centrifugation at 1000 rpm for 30 min at 4 °C. The supernatant with unbound GluOx was discarded. At lower amount of enzyme added, often a dark pellet from AuNPs aggregates would stick to the inter wall. 50 μL of the GluOx-AuNP conjugate pellets were collected at the bottom of a centrifuge tube and additional washing procedures using 10 mM sodium bicarbonate were repeated by adding a volume corresponding to the volume of the removed supernatant. This whole process was repeated a total of three times. To avoid artifacts in the size measurements of the conjugates, the $NaHCO_3$ buffer used for conjugate experiments was always filtered with 20 nm syringe filters before use.

Characterizing the Conditions for Enzyme Monolayer Coatings of AuNPs Using Flocculation Assay. To determine the molar ration of GluOx:AuNP added in solution, to start forming stable GluOx coverage onto the surface of AuNP, flocculation assay was performed using a Cary 4000 or Cary 5000 UV−vis spectrophotometry. The sample container is a Hellma quartz Suprasil cuvette QS 10 mm. The first step is similar to what was described for GluOx-AuNP conjugate synthesis process: after letting the mixture of GluOx and AuNP stay in the dark for 1.5 to 2 h, all samples except the bare AuNP in Milli-Q water (a control) NaCl was added with a 0.2 M final concentration and incubated for 20 min in the dark. The increased electrolyte concentration caused insufficiently coated GluOx-AuNP and uncoated AuNP to form Au aggregates. The bare AuNP has an absorption peak wavelength at around 524 nm, the sufficiently protected GluOx-AuNP conjugates are supposed to have the same absorption peak wavelength as that of AuNP, however, the absorption peak wavelength of Au aggregates formed from the insufficiently protected AuNP will shift to the red spectrum. Therefore, the minimal amount of enzyme needed to fully cover the AuNP surface can be determined by monitoring the UV−vis spectrum.

Measurements of GluOx-AuNP Conjugate Size. To determine the amount of GluOx needed to form a monolayer coating at the surface of the GluOx-AuNP conjugates with the aim to use the conditions of molar ratio enzyme:AuNP for coating the glutamate sensor with fully covering thin layer of enzyme, the resulting size of

DOI: 10.1021/acschemneuro.8b00624
ACS Chem. Neurosci. 2019, 10, 1744−1752

conjugates made at different ratios of GluOx:AuNP added in solution during the conjugation process were measured using Dynamic Light Scattering (DLS) and Nanoparticle Tracking Analysis (NTA). In the DLS measurements, a Zetasizer Nano ZS (Malvern Instruments Ltd., UK) equipped with a He−Ne laser 633 nm light source was used to measure the hydrodynamic diameter (D_{hyd}) of AuNPs and GluOx-AuNP conjugates. Each sample solution was put into a disposable, 70 μL BRAND cuvettes (BRAND GMBH + CO KG, Germany) with three measurements including 12−15 runs for every recording. A backscatter detection with angle of 173° at room temperature (22 °C) was used to detect the sample size. The Z-average size, that is an intensity mean via cumulate analysis, was reported and analyzed by Zetasizer Software 7.10. In the NTA measurements, a highly sensitive C11440−50B/A11893−02 sCMOS camera (Hamamatsu Photonics K.K., Japan) configured into a Malvern NanoSight LM10 (Malvern Instruments Ltd., UK) with a temperature-controlled sample chamber with a 488 nm (blue) laser was used to track the scattered light of individual AuNPs and GluOx-AuNP conjugates. The video of AuNPs and GluOx-AuNP conjugates under Brownian motion was captured by NTA 3.1 software and analyzed. Each measurement involves 5 runs where each run lasts for 60s and measurements were performed at room temperature (22 °C). All size measurements using NTA and DLS were carried out at approximately 6 h after the initiation of the conjugation process, when adding GluOx to AuNP in solution.

Preparation of 33 μm CFME. Carbon fiber microelectrodes (CFME) were prepared by aspirating single 33 μm diameter carbon fibers (Cytec Engineered Materials, Tempe, AZ) into borosilicate glass capillaries (1.2 mm O.D., 0.69 mm I.D., Sutter Instrument Co., Novato, CA). The filled capillaries were then pulled to a taper using a commercial micropipette puller (Model P-1000, Sutter Instrument Co., Novato, CA), and epoxy (Epoxy Technology, Billerica, MA) was used to seal the glass-carbon fiber junction of the electrode. The electrode tips were cut using a scalpel and polished at a 45° angle on a diamond dust-embedded micropipette beveling wheel (Narishige, Inc., London, U.K.). The electrodes were backfilled with silver paint or KCl (3 M), and a metal (tungsten or silver) wire was inserted as the connection to the potentiostat. All electrodes were tested in 1 mM FcMeOH by performing cyclic voltammetry between −0.2 V and +0.8 at 0.1 V s^{-1} with a saturated Ag/AgCl reference electrode (CH Instruments, U.S.A.) using a computer-controlled 1000C Series Multi-Potentiostat (CH Instruments, U.S.A.) to make sure the electrodes were well-functioning by evaluating their voltammograms prior to each experiment.

Functionalization of CFME Surface with AuNPs. Electrodes were functionalized with AuNP hemispheres by an electrochemical deposition similar to Finot et al.[36] with minor alterations regarding $HAuCl_4$ concentration and deposition time in order to optimize the AuNP size and electrode coverage on a 33 μm CFME, as earlier determined by our lab.[8] The CFME and an Ag/AgCl reference electrode were immersed into a solution of 0.5 mM $HAuCl_4$ and 500 mM H_2SO_4. A potential of +1.2 V was applied for 10 s followed by a potential of −0.6 V for 24 s via the 1000C Series Multi-Potentiostat (CH Instruments, U.S.A.). The AuNP surface area was then measured electrochemically by performing a linear sweep from +1.4 V (potential held for 5 s) to +0.5 V at a rate of 0.1 V s^{-1} in 500 mM H_2SO_4.[8] Here a $Cu/CuSO_4$ reference electrode was used instead of an Ag/AgCl reference electrode to avoid chloride contamination. The resulting peak at approximately +0.8 V was integrated by the inbuilt software in the 1000C Series Multi-Potentiostat and the obtained charge was divided with a factor of 489 μC cm^{-2} as used by Finot et al.[36]

Enzymes Monolayer Coating onto AuNP-CFME Glutamate Sensor Surface. A bottle of L-glutamate oxidase lyophilized powder (5 U) was filled with 500 μL of 10 mM sodium bicarbonate (pH 8.2) to completely dissolve the enzyme by gently rotating the bottle with the buffer solution. After determining the concentration of GluOx in solution using UV−vis measurement as described above and using the molar ratio of GluOx:AuNP needed in solution to fully coat the gold surface, as determined by flocculation assay, DLS, and NTA measurements, the tip of each AuNP-CFME was immersed into 100 μL of enzyme solution for approximately 2−3 h in room temperature where the GluOx self-adsorbed to the sensor surface. Most commonly, the GluOx-AuNP-CFME glutamate sensors were constructed immediately before use, or otherwise stored in phosphate-buffered saline (PBS) (10 mM, pH 7.2) at 4 °C for short periods of time before use within 1 day.

Characterization of the Glutamate Sensor Sensitivity and Selectivity. Detection of glutamate was performed by chronoamperometry in PBS using the computer-controlled a 1000C Series Multi-Potentiostat (CH Instruments, U.S.A.). Briefly, a constant potential, where no reactions occur (0 V), was applied to the glutamate sensor against a saturated Ag/AgCl reference electrode for 10 s followed by an immediate change to −0.5 V, where the reduction of the enzymatic product, hydrogen peroxide, was recorded. The amplitude of the resulting steady state reduction current achieved at −0.5 V versus the current at 0 V was determined 30 s after switching to the lower potential. A glutamate calibration curve was achieved by subjecting the sensor surface to glutamate solutions in a concentration range from 10 μM to 10 mM using freshly prepared solutions from a 1 M glutamate stock solution by adding aliquots of glutamate solution to a bulk PBS solution. The response of the following potential interfering analytes; acetylcholine, glutamine, dopamine, ascorbic acid, and glucose in 100 μM was also tested. In addition, the glutamate sensor was tested for the target analyte glutamate and for the main inference, dopamine, in a concentration range of from 10 μM to 1 mM using cyclic voltammetry. The current versus potential was recorded by scanning the potential between −0 V and −0.6 V versus a saturated Ag/AgCl reference electrode (CH Instruments, U.S.A.) at a 0.1 V s^{-1} scan rate using a Multi-Potentiostat (1000C Series, CH Instruments, U.S.A.). All solutions were bubbled with nitrogen gas to keep the O_2 concentration in solution to a low level during experiments.

Mouse Brain Slice Preparation. Male rodents (mice C57BL and rats Sprague−Dawley from Charles river, Sulzfeld, Germany) were housed in a 12-h light/dark cycle (light on at 0700 h) in group cages with *ad libitum* access to chow (Teklad Global 16% Protein Rodent Diet 2016, Envigo, Huntingdon, U.K.) and water. All rodents were aged between 4 and 8 weeks when sacrificed for amperometric recordings. They were anesthetized using isoflurane (Baxter Medical AB, Sweden), decapitated, and the brains were removed quickly in accordance with regulations of the Swedish Animal Welfare law and approved by the local ethical committee (ethics number 29-2014) for animal research at the University of Gothenburg, Sweden. Coronal slices containing NAc (400 μm) were cut in glycerol solution (at 3 °C) containing (in mM): glycerol, 219; KCl, 2.5, NaH_2PO_4, 1.2; $CaCl_2$, 1.2; $MgCl_2$, 7; $NaHCO_3$, 25; and glucose, 11 using Microtome HM 650 V, Thermo Fisher Scientific, Loughborough, U.K. Slices were then incubated at 30 °C for at least 45 min before recordings; the incubation medium contained (in mM): NaCl, 125; KCl, 2.5; NaH_2PO_4, 1.25; $NaHCO_3$, 25; $MgCl_2$, 4; $CaCl_2$, 1; D-Glucose, 10; and sucrose, 15. After they were incubated, slices were transferred to a submerged chamber and super fused with artificial cerebrospinal fluid (aCSF) (in mM): NaCl, 125; KCl, 2.5; $NaHCO_3$, 25; $CaCl_2$, 2.0; $MgCl_2$, 1.3; and D-Glucose, 10 at room temperature at a flow rate of 1 mL $minute^{-1}$. All solutions were aerated (5% carbon dioxide/95% oxygen) for at least 30 min prior to use, and aeration continued during recordings to keep a constant CO_2 and O_2 levels in solution.

Amperometric Recording of Glutamate Activity in Rodent Brain Slice. Before performing the ex vivo measurements, the functionality of GluOx-AuNP-CFME glutamate sensors was tested with 100 mM glutamate bulk solution (dissolved in aCSF) by chronoamperometry using a MultiClamp 700B (Molecule Devices, Sunnyvale, CA, U.S.A.). A constant potential of 0 V for 10 s was applied to the sensor surface versus a Ag/AgCl reference electrode and by lowering the applied potential to −0.5 V for 1 min, the steady state current amplitude shift was recorded. Each sensor was tested at the recording potential of −0.5 V before experiments, and only sensors that provided a current amplitude response that corresponded to the concentration of glutamate in solution were used for slice recordings. An upright Nikon E600FN (Nikon Inc., Japan) fluorescence microscope equipped with 4× lens and infrared−differential interference contrast was used for placing the glutamate

DOI: 10.1021/acschemneuro.8b00624
ACS Chem. Neurosci. 2019, 10, 1744−1752

sensor at the surface of the core region of the NAC in the brain slice. When inserted into the tissue, the sensor was then lowered to a depth of approximate 20 μm and the sensor tip remained visible by the microscope imaging. All recordings were limited to NAc core region of brain slice with an approximate angle of 45 deg to the plane of brain slice. Electrochemical recordings were performed by holding a constant potential of −0.5 V at the sensor surface versus a Ag/AgCl reference electrode using a MultiClamp 700B potentiostat (Molecule Devices, Sunnyvale, CA, U.S.A.). All signals were Bessel filtered at 10 kHz and digitalized at 20 kHz using a Digidata model 1440A with Axoscope 10.3.1.4 software (Molecule Devices, Sunnyvale, CA, U.S.A.), except for two measurements that were digitalized at 10 kHz and filtered at 4 kHz.

Data Analysis of Single Glutamate Exocytosis Events. The amperometric data were analyzed by a IgorPro 6.37 software developed by David Sulzer's group.[21] The data were smoothed at 5 kHz (binomial sm.) before analysis. The threshold for collecting spikes was 5 times that of the standard deviation of the noise. The amperometric trace was carefully visually checked, and false spikes were manually removed. In order to reduce the variance of the data, only current traces with more than 30 spikes were used in the analysis. All signals that were slower than 20 ms presented in two recordings were excluded from data analysis, assuming that these slower events might be related to extrasynaptic glutamate release from glial cells and astrocytes.[31,32] Current spike parameters were evaluated in terms of halftime ($T_{1/2}$) of a single exocytosis event was defined as the peak width at half-height of the peak. The rise time (T_{rise}) was defined as the measured rise time from 25% to 75% of the maximum peak height. The fall time (T_{fall}) was measured as the peak decay time from 75% to 25% of the maximum peak height. I_{max} was measured as the maximum current amplitude of each spike.

■ ASSOCIATED CONTENT

Supporting Information

The Supporting Information is available free of charge on the ACS Publications website at DOI: 10.1021/acschemneuro.8b00624.

Sensor characterization experiments (PDF)

■ AUTHOR INFORMATION

Corresponding Author

*E-mail: cans@chalmers.se.

ORCID

Ann-Sofie Cans: 0000-0002-3059-2399

Author Contributions

This project was conceived and designed by A-S.C, Y.W., J.B., D.M., and K.S., J.D.K took part in the initial development stage of the glutamate sensor concept. Y.W. performed the flocculation assays, DLS and NTA measurements, analyzed and prepared figures of these results. D.M. performed the brain slicing, and Y.W. and D.M performed the ex vivo electrochemical glutamate recordings in brain slices. Y.W. analyzed the ex vivo recording data and prepared figures of these results. J.B. characterized the sensor for selectivity and sensitivity; analyzed and prepared the figures of these results. Y.W. performed the selectivity experiment using cyclic voltammetry, analyzed and prepared a figure of the results. The authors Y.W, J.B and D.M wrote the first draft of this manuscript, K.S and A-S.C improved the manuscript further. All authors have read, discussed, and approved the final version of this manuscript.

Funding

We gratefully acknowledge financial support from The Swedish Research Council, The Swedish Brain Foundation, Ragnar Söderberg Foundation, The Novo Nordisk Foundation, The Wallenberg Center for Molecular and Translational Medicine at the University of Gothenburg, Ernst and Fru Rådman Colliander Stiftelse, Wilhelm and Martina Lundgren Stiftelse, and Magnus Bergvall Stiftelse.

Notes

The authors declare no competing financial interest.

■ ACKNOWLEDGMENTS

We thank Dr. Eric Hanse for use of microscope and low-current potentiostat.

■ ABBREVIATIONS

GluOx, glutamate oxidase; AuNP, gold nanoparticle; NAc, nucleus accumbens; DLS, dynamic light scattering; NTA, nanoparticle tracking analysis

■ REFERENCES

(1) Neurotransmitters. (2001) In *Neuroscience*, 2nd ed [Online]. Purves, D., Augustine, G. J., Fitzpatrick, D., Katz, L. C., LaMantia, A.-S., McNamara, J. O., and Williams, S. M., Eds.; Sinauer Associates, Sunderland, MA; Chapter 6. https://www.ncbi.nlm.nih.gov/books/NBK10807/.

(2) McEntee, W. J., and Crook, T. H. (1993) Glutamate: its role in learning, memory, and the aging brain. *Psychopharmacology (Berl). 111*, 391−401.

(3) Meldrum, B. S. (2000) Glutamate as a neurotransmitter in the brain: review of physiology and pathology. *J. Nutr. 130*, 1007S−15S.

(4) Djuricic, B. (2002) Glutamate in brain: transmitter and poison. *Glas. Srp. Akad. Nauka Med.*, 55−76.

(5) Sapolsky, R. (2005) *Biology and Human Behavior: The Neurological Origins of Individuality*, Biol. Hum. Behav. Neurol. Orig. Individ. 2nd ed., The Teaching Company, Chantilly, VA.

(6) Hascup, E. R., Hascup, K. N., Talauliker, P. M., Price, D. A., Pomerleau, F., Quintero, J. E., Huettl, P., Gratton, A., Strömberg, I., and Gerhardt, G. A. (2013) Sub-second measurements of glutamate and other neurotransmitter signaling using enzyme-based ceramic microelectrode arrays. *Neuromethods 80*, 179.

(7) Qiu, Q. F., Zhang, F. L., Tang, Y., Zhang, X. W., Jiang, H., Liu, Y. L., and Huang, W. H. (2018) Real-time Monitoring of Exocytotic Glutamate Release from Single Neuron by Amperometry at an Enzymatic Biosensor. *Electroanalysis 30*, 1054−1059.

(8) Keighron, J. D., Wigström, J., Kurczy, M. E., Bergman, J., Wang, Y., and Cans, A.-S. (2015) Amperometric detection of single vesicle acetylcholine release events from an artificial cell. *ACS Chem. Neurosci. 6*, 181−188.

(9) Caruso, F., and Schüler, C. (2000) Enzyme multilayers on colloid particles: Assembly, stability, and enzymatic activity. *Langmuir 16*, 9595−9603.

(10) Haupt, B., Neumann, T., Wittemann, A., and Ballauff, M. (2005) Activity of Enzymes Immobilized in Colloidal Spherical Polyelectrolyte Brushes. *Biomacromolecules 6*, 948−955.

(11) Shirayama, Y., and Chaki, S. (2006) Neurochemistry of the Nucleus Accumbens and its Relevance to Depression and Antidepressant Action in Rodents. *Curr. Neuropharmacol. 4*, 277−291.

(12) Phillipson, O. T., and Griffiths, A. C. (1985) The topographic order of inputs to nucleus accumbens in the rat. *Neuroscience 16*, 275−296.

(13) Zaczek, R., Hedreen, J. C., and Coyle, J. T. (1979) Evidence for a hippocampal-septal glutamatergic pathway in the rat. *Exp. Neurol. 65*, 145−156.

(14) Fuller, T. A., Russchen, F. T., and Price, J. L. (1987) Sources of presumptive glutamergic/aspartergic afferents to the rat ventral striatopallidal region. *J. Comp. Neurol. 258*, 317−338.

(15) Gorelova, N., and Yang, C. R. (1996) The course of neural projection from the prefrontal cortex to the nucleus accumbens in the rat. *Neuroscience 76*, 689−706.

DOI: 10.1021/acschemneuro.8b00624
ACS Chem. Neurosci. 2019, 10, 1744−1752

(16) Kalivas, P. W., and O'Brien, C. (2008) Drug addiction as a pathology of staged neuroplasticity. *Neuropsychopharmacology 33*, 166.
(17) Britt, J. P., Benaliouad, F., McDevitt, R. A., Stuber, G. D., Wise, R. A., and Bonci, A. (2012) Synaptic and Behavioral Profile of Multiple Glutamatergic Inputs to the Nucleus Accumbens. *Neuron 76*, 790−803.
(18) Kessler, M., Kiliman, B., Humes, C., and Arai, A. C. (2008) Spontaneous activity in Purkinje cells: Multi-electrode recording from organotypic cerebellar slice cultures. *Brain Res. 1218*, 54−69.
(19) Hermann, J., Pecka, M., von Gersdorff, H., Grothe, B., and Klug, A. (2007) Synaptic Transmission at the Calyx of Held Under In Vivo-Like Activity Levels. *J. Neurophysiol. 98*, 807−820.
(20) Schroeder, T. J., Jankowski, J. A., Kawagoe, K. T., Wightman, R. M., Lefrou, C., and Amatore, C. (1992) Analysis of diffusional broadening of vesicular packets of catecholamines released from biological cells during exocytosis. *Anal. Chem. 64*, 3077−3083.
(21) Mosharov, E. V., and Sulzer, D. (2005) Analysis of exocytotic events recorded by amperometry. *Nat. Methods 2*, 651.
(22) Watson, D. J., Gummi, R. R., Papke, J. B., and Harkins, A. B. (2011) Analysis of amperometric spike shapes to release vesicles. *Electroanalysis 23*, 2757−2763.
(23) Cragg, S. J., and Rice, M. E. (2004) DAncing past the DAT at a DA synapse. *Trends Neurosci. 27*, 270.
(24) Wightman, R. M., Schroeder, T. J., Finnegan, J. M., Ciolkowski, E. L., and Pihel, K. (1995) Time course of release of catecholamines from individual vesicles during exocytosis at adrenal medullary cells. *Biophys. J. 68*, 383−390.
(25) Majdi, S., Berglund, E. C., Dunevall, J., Oleinick, A. I., Amatore, C., Krantz, D., and Ewing, A. G. (2015) Electrochemical Measurements of Optogenetically Stimulated Quantal Amine Release from Single Nerve Cell Varicosities in Drosophila Larvae. *Angew. Chem., Int. Ed. 54*, 13609−13612.
(26) Grabner, C. P., and Zenisek, D. (2013) Amperometric Resolution of a Prespike Stammer and Evoked Phases of Fast Release from Retinal Bipolar Cells. *J. Neurosci. 33*, 8144−8158.
(27) Chapochnikov, N. M., Takago, H., Huang, C. H., Pangršič, T., Khimich, D., Neef, J., Auge, E., Göttfert, F., Hell, S. W., Wichmann, C., Wolf, F., and Moser, T. (2014) Uniquantal release through a dynamic fusion pore is a candidate mechanism of hair cell exocytosis. *Neuron 83*, 1389−1403.
(28) Ren, L., Mellander, L. J., Keighron, J., Cans, A.-S., Kurczy, M. E., Svir, I., Oleinick, A., Amatore, C., and Ewing, A. G. (2016) The evidence for open and closed exocytosis as the primary release mechanism. *Q. Rev. Biophys. 49*, e12.
(29) Albillos, A., Dernick, G., Horstmann, H., Almers, W., Alvarez de Toledo, G., and Lindau, M. (1997) The exocytotic event in chromaffin cells revealed by patch amperometry. *Nature 389*, 509−512.
(30) Bokvist, K., Holmqvist, M., Gromada, J., and Rorsman, P. (2000) Compound exocytosis in voltage-clamped mouse pancreatic β-cells revealed by carbon fibre amperometry. *Pfluegers Arch. 439*, 634−645.
(31) Angulo, M. C., Kozlov, A. S., Charpak, S., and Audinat, E. (2004) Glutamate released from glial cells synchronizes neuronal activity in the hippocampus. *J. Neurosci. 24*, 6920−6927.
(32) Fellin, T., Pascual, O., Gobbo, S., Pozzan, T., Haydon, P. G., and Carmignoto, G. (2004) Neuronal synchrony mediated by astrocytic glutamate through activation of extrasynaptic NMDA receptors. *Neuron 43*, 729−743.
(33) Clay, M., and Monbouquette, H. G. (2018) A Detailed Model of Electroenzymatic Glutamate Biosensors To Aid in Sensor Optimization and in Applications in Vivo. *ACS Chem. Neurosci. 9*, 241−251.
(34) Hermann, J., Pecka, M., von Gersdorff, H., Grothe, B., and Klug, A. (2007) Synaptic Transmission at the Calyx of Held Under In Vivo-Like Activity Levels. *J. Neurophysiol. 98*, 807−820.
(35) Kusakabe, H., Midorikawa, Y., Fujishima, T., Kuninaka, A., and Yoshino, H. (1983) Purification and properties of a new enzyme, l-glutamate oxidase, from streptomyces sp. X-119−6 grown on wheat brant. *Agric. Biol. Chem. 47*, 1323−1328.
(36) Finot, M. O., Braybrook, G. D., and Mcdermott, M. T. (1999) Characterization of electrochemically deposited gold nanocrystals on glassy carbon electrodes. *J. Electroanal. Chem. 466*, 234−241.

DOI: 10.1021/acschemneuro.8b00624
ACS Chem. Neurosci. 2019, 10, 1744−1752